Laser-induced breakdown spectroscopy of bulk aqueous solutions at oceanic pressures: evaluation of key measurement parameters

Anna P. M. Michel, Marion Lawrence-Snyder, S. Michael Angel, and Alan D. Chave

The development of *in situ* chemical sensors is critical for present-day expeditionary oceanography and the new mode of ocean observing systems that we are entering. New sensors take a significant amount of time to develop; therefore, validation of techniques in the laboratory for use in the ocean environment is necessary. Laser-induced breakdown spectroscopy (LIBS) is a promising *in situ* technique for oceanography. Laboratory investigations on the feasibility of using LIBS to detect analytes in bulk liquids at oceanic pressures were carried out. LIBS was successfully used to detect dissolved Na, Mn, Ca, K, and Li at pressures up to 2.76×10^7 Pa. The effects of pressure, laser-pulse energy, interpulse delay, gate delay, temperature, and NaCl concentration on the LIBS signal were examined. An optimal range of laser-pulse energies was found to exist for analyte detection in bulk aqueous solutions at both low and high pressures. No pressure effect was seen on the emission intensity for Ca and Na, and an increase in emission intensity with increased pressure was seen for Mn. Using the dual-pulse technique for several analytes, a very short interpulse delay resulted in the greatest emission intensity. The presence of NaCl enhanced the emission intensity for Ca, but had no effect on peak intensity of Mn or K. Overall, increased pressure, the addition of NaCl to a solution, and temperature did not inhibit detection of analytes in solution and sometimes even enhanced the ability to detect the analytes. The results suggest that LIBS is a viable chemical sensing method for *in situ* analyte detection in high-pressure environments such as the deep ocean.

OCIS codes: 010.4450, 140.3440, 300.6360.

1. Introduction

Since laser-induced breakdown spectroscopy (LIBS) was first reported in 1962, the technique has evolved into a widely used method for laboratory analytical chemistry.[1–8] Due to several advantages over other methods, LIBS has been identified as a viable tool for *in situ* measurements, especially in extreme environments.[9,10] The technique yields simultaneous sensitivity to virtually all elements in the parts-per-million (ppm) or better range in solids, gases, aerosols, and at the gas–liquid interface. LIBS is effectively noninvasive, requiring only a small sample (typically, picograms to nanograms of material are ablated). Unlike for many analysis techniques, the sample does not need to be prepared. LIBS requires only optical access to a sample and therefore can be used in a stand-off mode without perturbing the sample environment. LIBS measurements are essentially real time, with typical sampling rates of less than 1 per second. These characteristics are all required for *in situ* chemical sensing in the ocean.[11–15]

Although researchers have been successful at inducing plasma ablation on submerged materials,[16] on a water surface or film,[17–22] and in liquid jets, droplets, and flowing solutions,[23–29] only limited LIBS work has focused on analyte detection within bulk aqueous solutions.[30–32] Furthermore, the work within bulk aqueous solutions has been at atmospheric pressure. Pioneering work by Cremers *et al.*[30] showed that LIBS could identify Li, Na, K, Rb, Cs, Be, Ca, B, and Al

A. P. M. Michel (amichel@whoi.edu) is with the Department of Applied Ocean Physics and Engineering, Massachusetts Institute of Technology/Woods Hole Oceanographic Institution Joint Program, Woods Hole Oceanographic Institution, Mail Stop #7, Woods Hole, Massachusetts 02543. M. Lawrence-Snyder and S. M. Angel are with the Department of Chemistry and Biochemistry, University of South Carolina, Columbia, South Carolina 29208. A. D. Chave is with the Department of Applied Ocean Physics and Engineering, Woods Hole Oceanographic Institution, Mail Stop #7, Woods Hole, Masssachusetts 02543.

Received 24 July 2006; revised 28 December 2006; accepted 2 January 2007; posted 4 January 2007 (Doc. ID 73334); published 9 April 2007.

0003-6935/07/132507-09$15.00/0

in aqueous solutions with varying detection limits, but typically at the parts-per-million level. Several studies in bulk liquids have displayed a reduction in the time during which plasma emission can be observed as compared to that in air.[16,30,31,33] The plasma lifetime is typically ≤ 1 μs in bulk liquids, whereas at an air–liquid interface it averages 5–20 μs. Laser-induced plasmas formed in solution are also characterized by a reduction in plasma light intensity.

The effects of elevated pressure and temperature on LIBS spectra have received limited attention. Although a few researchers report on LIBS at superatmospheric pressures, they do not extend beyond 1×10^7 Pa (note: 1 Pa = 1×10^{-5} bars), which is well below the ambient pressure in the deep ocean[10,34]; yet, none of these studies were for liquids. Although, we have previously reported preliminary findings that show the ability to detect analytes in high-pressure bulk aqueous solutions,[35] we now focus on the key measurement parameters that are needed for analyte detection. The influence of *in situ* temperature is anticipated to be weak because of the high plasma temperature (≈8000 K at early times).[36–39]

For many years, oceanography has been in an expeditionary mode where research vessels are used for short-term instrument deployments with limited resolution in time. Although oceanographers will continue to study the ocean in this way, a new paradigm using ocean observatories for long-term *in situ* observing is upon us. As this shift toward long-term ocean observing systems becomes recognized, we must also acknowledge the need for *in situ* sensors, especially those capable of temporal studies. A major need is for chemical sensors. The development of new sensors for oceanography takes a significant amount of time, and hence laboratory validation of techniques such as LIBS is necessary now to identify techniques that are viable for chemical detection in high-pressure, high-salinity, aqueous environments.

Although LIBS has the potential for use in numerous ocean environments and has applicability to solids and liquids, we have focused on the feasibility of detecting elements at one extreme ocean environment, hydrothermal vents. Hydrothermal venting occurs on mid-ocean ridges where seawater circulates through the fractured and permeable oceanic crust. Exit temperatures at discrete (orifice diameters of a few centimeters) high-temperature vents range from 200 °C to 405 °C at ambient pressures of 1.5×10^7 to 3.7×10^7 Pa. Low-temperature (usually <35 °C) diffuse flow seeping from porous surfaces or cracks is frequently observed.[40] The circulation is driven by the direct or indirect thermal effects of magma at subseafloor depths of up to a few kilometers. Substantial changes in fluid composition occur due to interaction with the host rock, phase separation into a mixed liquid–vapor form, and possibly magma degassing. Many alkalis (e.g., Li, Na, and Ca) and transition metals (e.g, Fe, Mn, Cu, and Zn) are leached from the host rock and concentrated to varying degrees in the hydrothermal fluid, while Mg and SO_4 are largely removed from the fluid by precipitation into Mg-OH-Si minerals and anhydrite, respectively.[40] Von Damm[40] and Butterfield *et al.*[41] provide comprehensive reviews of the chemistry of hydrothermal vent fluids.

In this paper, we explore the effect of vent system environmental factors such as pressure, temperature, and NaCl concentration on the LIBS signal to assess the feasibility of developing LIBS for *in situ* chemical sensing in the ocean. In addition, several system parameters (laser energy per pulse, interpulse spacing, and gate delay) are optimized for high pressures for the first time, to the best of our knowledge.

2. Experiment

A laboratory LIBS system was designed to operate with a high-pressure cell (Fig. 1). For single-pulse experiments, a Continuum Surelite III laser (5 ns pulse width) was utilized. For dual-pulse experiments, a Quantel Nd 580 (9 ns pulse width) was used for the first laser pulse followed by a second pulse from the Surelite laser. Both lasers were *Q*-switched Nd:YAG types operated at the fundamental wavelength with a repetition rate of 5 Hz. For dual-pulse experiments, a variable clock (Stanford Instruments Model SR250) and a delay generator (Stanford Instruments Model DG535) controlled laser triggering.

The laser pulses were focused into a high-pressure cell, designed to reach pressures of 3.45×10^7 Pa and constructed of stainless-steel Swagelok fittings with six 1 in.-i.d. (inside diameter) (1 in. = 2.54 cm) and one 0.25 in.-o.d. (outside diameter) ports. Stainless-steel tubing (0.125 in.) connected one port to a pump (Isco Syringe Pump Model 260D, Teledyne Technologies Incorporated) that allowed aqueous solutions to flow into the cell and the cell to be pressurized. A second port was equipped with the same tubing and a regulating valve for cell drainage. Two ports were fitted with 1 in. diam, 0.125 in. thick circular sapphire windows (MSW100/125, Meller Optics Incorporated) held in place by hex nuts and sealed with

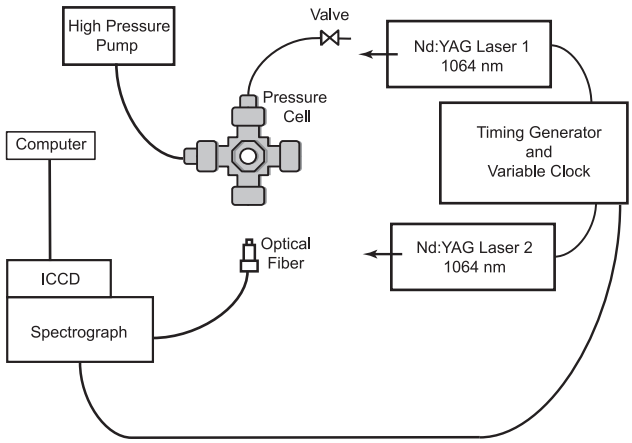

Fig. 1. Schematic of the laboratory LIBS apparatus. Note that in the drawing, the laser pulses are simply represented by arrows as their optical paths are described in Fig. 2.

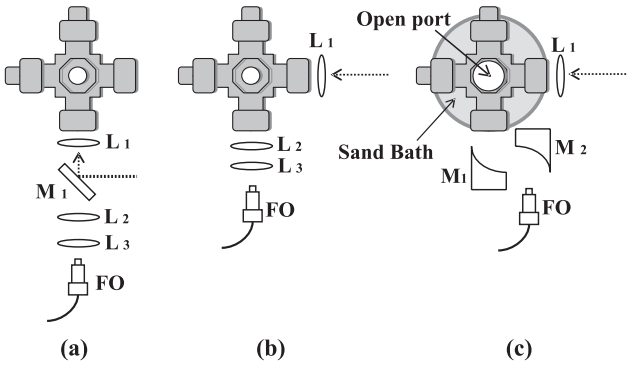

Fig. 2. Optical arrangements used in experiments showing the high-pressure cell with respect to incoming laser pulses (signified by a dashed line). FO = optical fiber (a) L_1, L_2, and $L_3 = f/4$ lenses; M_1 = dielectric coated mirror. (b) $L_1 = f/4$. To study the effect of NaCl concentration on spectra: $L_2 = f/3$ lens, $L_3 = f/2$ lens. To study the detection of Ca at varying concentrations: $L_2 = f/4$ lens, $L_3 = f/3$ lens. (c) $L_1 = f/4$, M_1 and M_2 = parabolic off-axis mirrors.

rubber washers, allowing 0.75 in. of each window to be visible outside the cell. The remaining two ports were sealed with Swagelok plugs (SS-1610-P).

Three different optical arrangements for focusing the laser pulses into the cell and for collection of the plasma emission were used in these experiments, as detailed in Fig. 2. Because the purpose of these experiments was initial investigation into the feasibility of using LIBS for ocean applications, one of the goals was determining the best optical setup. For dual-pulse operation, the lasers were collinear. In some single-pulse configurations, light collection was collinear to the laser pulse, while in others it was orthogonal for ease of alignment. All optics were mounted on micrometer stages, enabling precise control of beam overlap and collection field of view within the high-pressure cell. All lenses were made of fused silica.

In all optical configurations, the plasma emission was focused on a 2 mm core diameter, 0.51 NA light guide (Edmund Scientific Model 02551). The light guide was connected to a 0.25 m, $f/4$ spectrograph (Chromex Model 250is/RF) with a 1200 groove/mm grating blazed at 500 nm. The slit width (W) ranged from 25 to 250 μm. Data were collected on an intensified CCD detector (Princeton Instruments, I-Max 1024E) and acquired with a computer running WinSpec/32 software. All spectra were accumulations of 250 shots at the maximum gain setting of 255. All error bars represent $\pm 1\sigma$. A similar apparatus and setup was previously used to demonstrate the feasibility of high-pressure LIBS.[35]

The key LIBS timing parameters have been previously described.[16,32] The first and second laser pulse energies are referred to as E_1 and E_2. For dual-pulse experiments, the time interval between the two pulses or interpulse delay is referred to as ΔT. The gate delay, t_d, is the time between the last laser pulse and the turn-on of the detector. The plasma emission is recorded by the detector for the length of time set by the gate width, t_b, which was set at 1 μs for all the experiments reported here.

Laser-beam-waist width d_{σ_0} can be estimated by

$$d_{\sigma_0} = \frac{4f\lambda M^2}{\pi D}, \tag{1}$$

where f is the focal length of the focusing lens (100 mm), λ is the laser wavelength (1064 nm), M^2 is the beam propagation ratio, which is typically 2:10 for Nd:YAG lasers (we use a value of 6), and D is the diameter of the illuminated aperture of the focusing lens (≈25 mm).[42] The beam-waist width for the system is approximately 0.03 mm. The average irradiance (I_f) at the beam waist can be estimated using

$$I_f = \frac{\pi E_L D^2}{4\tau_L f^2 \lambda^2 M^4}, \tag{2}$$

where E_L is the laser-pulse energy and τ_L is the pulse duration at the FWHM[42] (for the Continuum laser, $\tau_L = 5$ ns, and for the Quantel laser, $\tau_L = 9$ ns). The pulse energies of the Continuum laser used vary between ≈10 and 100 mJ. The irradiance of the beam at the beam waist thus varies from $\approx 2.4 \times 10^{11}$ to $\approx 2.4 \times 10^{12}$ W/cm^2. The pulse energies of the Quantel laser used vary between ≈10 and 125 mJ with the irradiance thus varying from 1.3×10^{11} to 1.7×10^{12} W/cm^2.

Sample solutions were made by dissolving NaCl, $CaCl_2$, LiCl, and $MnSO_4 \cdot H_2O$ in deionized water. Where noted, NaCl was added to the solutions to simulate a seawater environment. All concentrations are listed in parts per million (ppm wt./vol.).

3. Results and Discussion

A. Effect of Pulse Energy on LIBS Emission

1. *Single-Pulse LIBS*

Two key constraints on the design of an oceanographic sensor system are instrument power consumption and form factor, both of which must be minimized. LIBS operation with a small, low-power laser would simplify the design of an oceanographic LIBS instrument. The effect of pulse energy on signal intensity for analytes in solution at elevated pressure was investigated with the goal of minimizing power consumption. The peak signal intensity for four analytes (Li, Ca, Na, and Mn) was measured at laser-pulse energies ranging from 11 to 91 mJ at both low (7×10^5 Pa) and high (2.76×10^7 Pa) pressures using the collinear optical configuration shown in Fig. 2(a) ($t_d = 350$ ns, $W = 75$ μm for Na, Mn, and Ca studies, and $W = 250$ nm for Li). Ten spectra were recorded and averaged for each condition.

Figure 3 shows the dependence of the Na(I) (588.995 nm) emission line on laser-pulse energy for 100 ppm Na. In both low- and high-pressure experiments, as pulse energy increases, a corresponding increase in

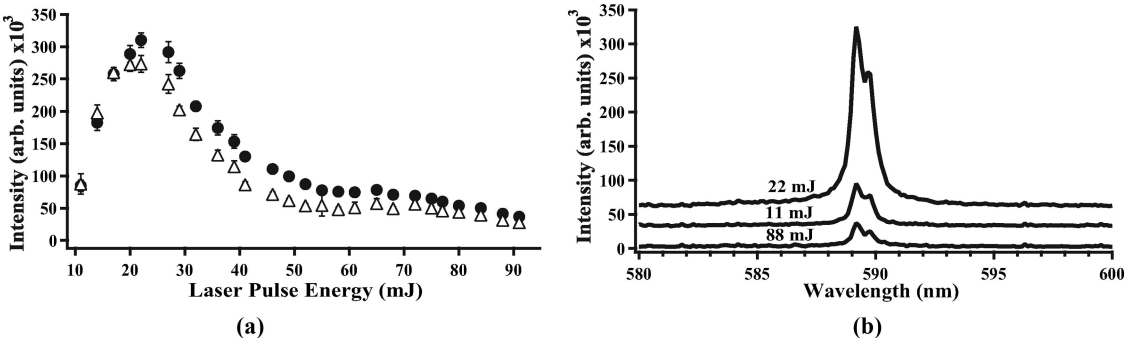

Fig. 3. Effect of laser pulse energy on the LIBS signal intensity of 100 ppm Na(I) (588.995 nm). (a) Data taken at 7×10^5 Pa (●) and 2.76×10^7 Pa (△). (b) Na(I) spectra taken at 2.76×10^7 Pa. Spectra offset for clarity.

peak intensity occurs until a maximum intensity is reached at 22 mJ [Fig. 3(a)]. Above this value, emission intensity decreases sharply up to ≈50 mJ, above which a more gradual decrease with energy is observed. These data suggest that, independent of pressure, a low laser-pulse energy yields greater emission intensity providing the energy exceeds a threshold value. Figure 3(b) compares spectra taken at laser-pulse energies below, above, and in the optimal energy range for Na. The top trace (22 mJ) shows a significantly greater intensity than at either a very low (middle trace, 11 mJ) or a high- (bottom trace, 88 mJ) pulse energy.

The effect of laser-pulse energy on Ca (422.673 nm) and Li (670.776 and 670.791 nm, unresolved doublet) emission displayed similar trends. When less than 14 mJ was used, Ca was virtually undetectable. As the pulse energy was increased above this level, emission intensified until a maximum was achieved at 36 mJ for low pressure (7×10^5 Pa) and at 29 mJ for high pressure (2.76×10^7 Pa). This range for both the low- and the high-pressure environments was ≈25–50 mJ. At energy levels beyond the optimal range, intensity decreased slowly with increasing pulse energy, possibly due to plasma shielding. Plasma shielding occurs when the plasma itself reduces the transmission of the laser-pulse energy along the beam path. Calcium displayed a more gradual increase and then decrease in intensity and a wider range of optimal energy compared with Na. Similar trends were observed for Li. At both low and high pressures, plasma emission was not detectable below 11 mJ. At higher pulse energies and both pressures, the emission maximum was recorded at 27 mJ, above which a sharp decrease in intensity to 46 mJ was observed, followed by flattening to 72 mJ.

The relationship between emission intensity and laser-pulse energy for the unresolved 403 nm Mn(I) triplet was slightly different from the other three analytes. Figure 4(a) shows that the lowest laser-pulse energy (11 mJ) resulted in the highest emission intensity. At pulse energies greater than 11 mJ, the emission intensity gradually decreased until it was no longer detectable above ≈40 and ≈70 mJ for low and high pressures, respectively. The peak intensity was greater at high rather than at low pressure. Figure 4(b) compares spectra taken at 11, 22, and 88 mJ at 2.76×10^7 Pa.

The data for Na, Ca, Li, and Mn suggest that the pulse energy required to optimize the LIBS signal is analyte dependent due to different ionization energies but is minimally pressure dependent. A pulse energy threshold is also observed. For the four analytes studied, a relatively low laser-pulse energy (less than 50 mJ) produced the greatest signal intensity. A low-energy optimal range may exist due to effects from plasma shielding or moving breakdown. Plasmas can expand back along the laser beam path toward the laser resulting in elongated plasmas.[43] A higher-energy pulse may form a more elongated

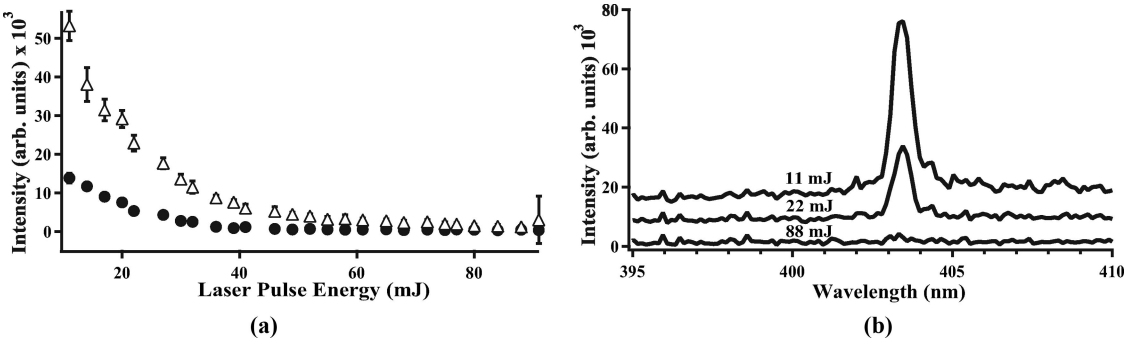

Fig. 4. Effect of laser pulse energy on the LIBS emission intensity of the unresolvable Mn(I) triplet (403 nm) (5000 ppm Mn in 2540 ppm NaCl). (a) Data taken at 7×10^5 Pa (●) and 2.76×10^7 Pa (△). (b) Mn(I) spectra taken at 2.76×10^7 Pa. Spectra offset for clarity.

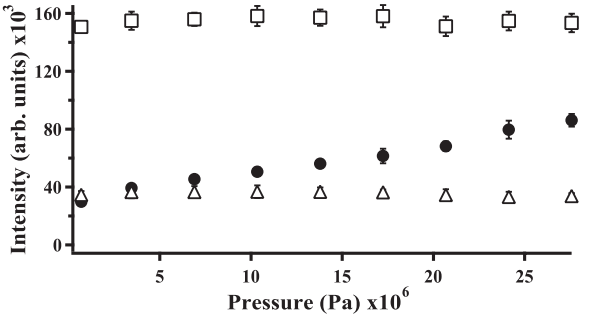

Fig. 5. Effect of pressure on LIBS emission intensity. □ = 100 ppm Na (588.995 nm) with E = 22 mJ; ● = 5000 ppm Mn (403 nm unresolvable triplet) with 2540 ppm NaCl, E = 14 mJ; △ = 500 ppm Ca (422.673 nm) with 2540 ppm NaCl, E = 20 mJ.

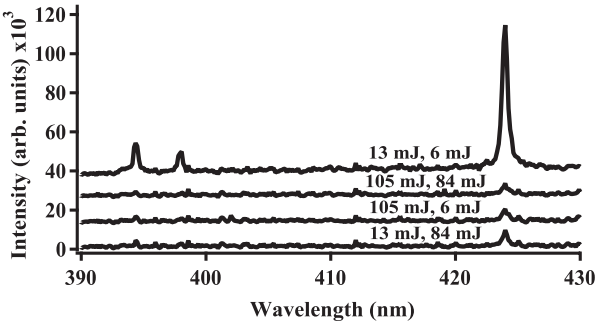

Fig. 6. Spectra of 1000 ppm Ca with 2540 ppm NaCl at 2.76 $\times$ 10^7 Pa under four dual-pulse conditions.

plasma or a series of plasmas as the breakdown threshold of the liquid is exceeded before the pulse reaches the focal point. This may result in nonoptimal collection of the plasma emission. Further studies using imaging techniques are needed to elucidate the effect of pulse energy on the plasma.

Figure 5 shows the effect of pressure on the LIBS signal for Na (588.995 nm), Mn (403 nm unresolvable triplet), and Ca (422.673 nm) using a low-energy single pulse. The gate delay was fixed at 350 ns and the slit width was fixed at 75 μm. Na and Ca display no change in signal intensity with increasing pressure, but Mn shows an increase. For all analytes examined, the FWHM did not change with pressure. Pressure under oceanic conditions does not induce a deleterious effect on signal intensity or on FWHM.

In these single-pulse energy experiments, the same gate delay and gate width were used for all energy levels and pressures. As discussed later in this paper, optimal gate delay may be energy dependent. Optimal gate width was not investigated and may be pressure and/or energy level dependent. As a result, the selected gate width and gate delay may influence the measured emission intensity. Optimal gate delay could also be analyte dependent, and hence a different gate delay could yield another trend with pulse energy. However, the selected conditions demonstrate that low-energy single laser pulses at high pressures are viable for measuring analytes in bulk aqueous liquids. This is promising toward the development of an ocean-going instrument where a small, low-power laser will be critical.

2. *Dual-Pulse LIBS at High Pressure*

An evaluation of dual-pulse LIBS for high-pressure bulk solutions shows that analyte detection is highly dependent on the interpulse delay. If the interpulse delay is short ($\ll$1 μs), signal intensity is greatly enhanced when compared with that measured using longer delay times. However, such a small interpulse delay may not be sufficient for a cavitation bubble to fully form before the second laser pulse creates a spark. Dual-pulse LIBS has been shown to enhance the signal intensity for some analytes in bulk aqueous solutions at atmospheric pressure.[30,32] However, such enhancements using longer interpulse delay times do not occur for high-pressure liquids.

To demonstrate the coupled effect of interpulse delay and pulse energy on emission intensity, four energy-level conditions were compared for four analytes at high pressure (2.76 $\times$ 10^7 Pa) over a range of interpulse delay times. The four conditions were (1) low E_1, low E_2 (low–low), (2) high E_1, high E_2 (high–high), (3) low E_1, high E_2 (low–high), and (4) high E_1, low E_2 (high–low) and are detailed in Table 1 (t_d = 350 ns, t_b = 1 μs). These experiments were completed using the optical configuration shown in Fig. 2(a).

For Ca (W = 100 μm), using a low E_1 followed by a low E_2 resulted in the highest peak intensity, possibly because when summed they give a low total energy (Fig. 6). The greatest emission is observed for E_1 = 13 mJ and E_2 = 6 mJ and yields the ionic Ca peaks (393.366 and 396.847 nm in addition to the atomic peak 422.673 nm). For this low–low condition, Fig. 7(a) shows the emission intensity change with ΔT. For ΔT greater than 1 μs, the intensity remained

Table 1. Conditions Used to Study the Effect of Dual-Pulse Energies on LIBS Emission

	Low E_1	Low E_2	High E_1	High E_2	Low E_1	High E_2	High E_1	Low E_2
	E_1 (mJ)	E_2 (mJ)	E_1 (mJ)	E_2 (mJ)	E_1 (mJ)	E_2 (mJ)	E_1 (mJ)	E_2 (mJ)
1000 ppm Ca, 2540 ppm NaCl	13	6	105	84	13	84	105	6
100 ppm Li	31	20	105	84	31	84	105	20
100 ppm Na	13	6	105	84	13	84	105	6
5000 ppm Mn, 2540 ppm NaCl	13	6	105	84	13	84	105	6

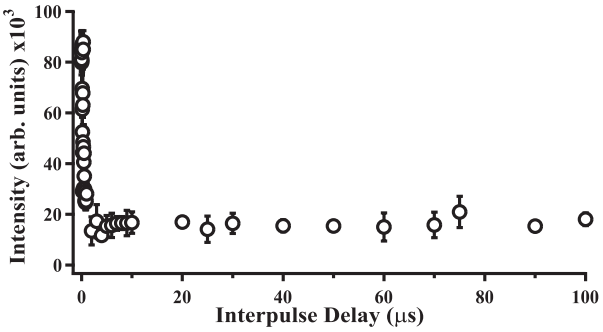

(a)

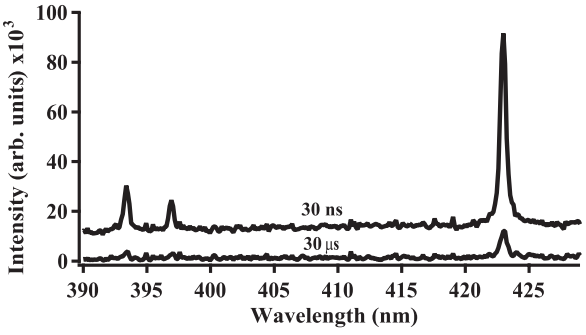

(b)

Fig. 7. (a) Effect of dual laser-pulse energies on emission intensity at 2.76×10^7 Pa for 1000 ppm Ca in 2540 ppm NaCl at various interpulse delays. Each data point is the average of five spectra. (b) Spectra of Ca showing the enhancement in signal for ΔT = 30 ns over ΔT = 30 μs. For (a) and (b): E_1 = 13 mJ, E_2 = 6 mJ.

stable at a value of 1.5×10^4 arb. units. For ΔT less than 1 μs, the low–low configuration yielded intensities between 2.5×10^4 and 8.7×10^4 arb. units. Figure 7(b) compares spectra at very short (30 ns—upper trace) to long (30 μs—lower trace) ΔT values. When a short ΔT is used, three Ca peaks [Ca(II) 393.366 nm, Ca(II) 396.847 nm, and Ca(I) 422.673 nm] are visible, while for long ΔT, only the Ca(I) peak is present with a much lower intensity. When ΔT is 30 ns, the low–low configuration yields significantly greater emission intensity than the other pulse energy configurations. For Li (W = 250 μm), a low E_1 followed by a low E_2 resulted in the greatest emission intensity. Table 2 shows peak emission for Li for four different dual-pulse conditions for ΔT between 50 ns and 1 μs. A small delay time (<1 μs) enhanced the emission as compared with a longer delay time when the low–high and low–low energy levels were used. For Na(I), the low–high and low–low conditions

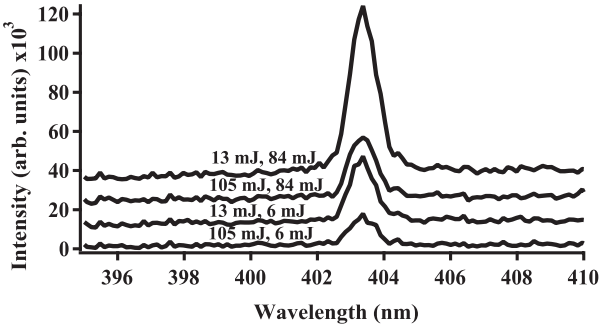

Fig. 8. Spectra of 5000 ppm Mn with 2540 ppm NaCl at 2.76×10^7 Pa under four dual-pulse conditions. The highest emission intensity is observed for a low–high pulse combination.

yielded similar intensities at all delay times, with maximum values of 9.3×10^5 and 8.3×10^5 arb. units, respectively, (W = 75 μm). After these four runs were compared, an additional configuration consisting of a 13 mJ first pulse followed by a 22 mJ second pulse was tested as a low–low dual-pulse condition with a slightly increased second-pulse energy. This resulted in peaks with intensities of 2.4×10^6 to 2.9×10^6 arb. units for all ΔT values between 10 ns and 100 μs, suggesting again that a low–low energy condition produces the greatest emission intensity. For Mn (W = 250 μm), at all interpulse delay times between 20 ns and 100 μs, a low E_1 followed by a high E_2, resulted in the highest emission intensity (Fig. 8).

These results show that the best dual-pulse conditions vary by analyte. However, it is important to note that, at high pressure, very short interpulse spacing results in a higher signal intensity than when dual pulses are separated by a more significant delay in time. The need for such rapid firing of the two pulses is only accomplished using two independent lasers instead of firing one laser rapidly. Two pulses separated by a short ΔT approaches single-pulse conditions, suggesting that dual-pulse LIBS may not be advantageous at elevated pressure.

B. Interrelationship of Pulse Energy, Gate Delay, and Pressure for Lithium

Emission intensity was recorded for the unresolved Li(I) doublet (670.776 and 670.791 nm) at two single-pulse energies (27 and 68 mJ) at both low (7×10^5 Pa) and high pressure (2.76×10^7 Pa) over a range of gate delays (0.1–3.7 μs) (t_b = 1 μs, W = 25 μm) using the optical configuration of Fig. 2(a). Comparing the two curves in Fig. 9, it is clear that a short gate delay should be used to enhance emission intensity. These

Table 2. Dual-Pulse Emission Intensity (arb. units)

	Condition 1	Condition 2	Condition 3	Condition 4
	Low E_1, Low E_2	High E_1, High E_2	Low E_1, High E_2	High E_1, Low E_2
100 ppm Li	2.5×10^5 to 3.7×10^5	2×10^4 to 7×10^4	5×10^4 to 1.5×10^5	1.5×10^4 to 5.3×10^4
5000 ppm Mn, 2540 ppm NaCl	4×10^3 to 4.2×10^5	2.1×10^5 to 5×10^5	7×10^5 to 8.3×10^5	1.6×10^3 to 2.6×10^5

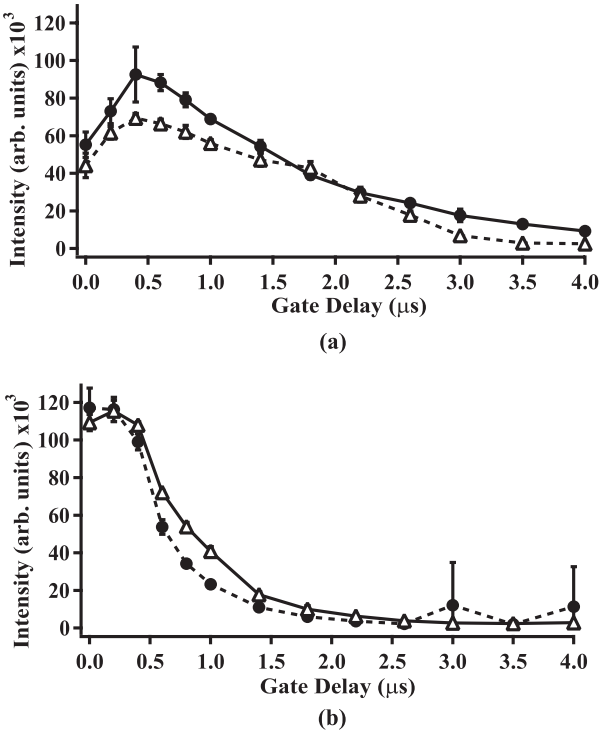

Fig. 9. Effect of gate delay on the LIBS signal for 1000 ppm Li (670 nm unresolvable doublet). ● = 7×10^5 Pa, △ = 2.57×10^7 Pa. (a) Data taken with a single low-energy pulse (27 mJ) and (b) with a single high-energy pulse (68 mJ).

results also suggest that the optimal gate delay may be pulse energy, but not pressure dependent.

C. Effect of NaCl Concentration on LIBS Spectra

Understanding how pervasive Na and Cl ions in solution affect the detection of other analytes is important for assessing the feasibility of using LIBS in the ocean, where the nominal concentrations of Na and Cl are 1.08×10^4 and 1.95×10^4 ppm, respectively.[44] Cremers *et al.* previously reported a decrease in the intensity ratio of Ca(II)/Ca(I) with the addition of NaCl.[30] The peak signal intensity for three analytes (1000 ppm Ca, 100 ppm Mn, and 1000 ppm K) was compared in three solutes: (1) deionized water, (2) 2540 ppm NaCl dissolved in deionized water, and (3) 25,400 ppm NaCl dissolved in deionized water using the optical configuration of Fig. 2(b) and for a range of pressures (3×10^5, 7×10^5, 1.7×10^6, 3.4×10^6, 6.9×10^6, 1.38×10^7, 2.07×10^7, 2.76×10^7 Pa). These studies were carried out with $E_1 = 40$ mJ, $E_2 = 125$ mJ, $\Delta T = 46$ ns, $W = 35$ μm, and $t_d = 100$ ns for Ca and K and $t_d = 200$ ns for Mn. The addition of NaCl significantly increased the emission intensity of the 422.673 nm Ca(I) atomic line whereas no significant effect was seen on the 393.366 and 396.847 nm Ca(II) ionic lines (Fig. 10). The signal-to-noise ratio for the Ca(II) ionic lines showed no significant change with the addition of NaCl, whereas the signal-to-noise ratio of Ca(I) increased from 22 to 30 with the addition of NaCl. The same increase was seen with the addition of 254 ppm NaCl and 25,400 ppm NaCl. In atomic emission, adding an easily ionizable element, for example, Na, can suppress ionization of other elements. This suggests that ionization suppression by Na increases the Ca(I) emission relative to the Ca(II) lines. No intensity change was seen for Mn(I) (403 nm unresolvable triplet) or K(I) (766.491 and 769.897 nm). However, since only atomic lines were detectable for Mn and K, the relative increase of atomic to ionic lines could not be compared.

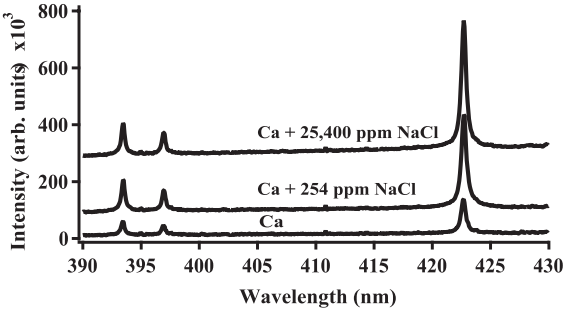

Fig. 10. Effect of the addition of NaCl in solution on spectra of 1000 ppm Ca at 2.57×10^7 Pa.

These two outcomes (enhancement of the signal or no change to the signal) suggest that the high NaCl concentration in the ocean will not have a deleterious effect on the ability to detect Ca, Mn, and K analytes. It also suggests that further work is needed to elucidate the effect NaCl has on other analytes.

D. Detection of Calcium at Varying Concentrations

Ca was used to determine whether increased pressure affects the limit of detection. Five pressures ranging from 7×10^5 to 2.76×10^7 Pa were investigated at concentrations ranging from 10 to 5000 ppm in a solution containing several analytes (69 ppm Br, 10,828 ppm Na, 89 ppm Fe, 958 ppm K, 46 ppm Mn, 18,932 ppm Cl in DI water) found in hydrothermal vent fluids at representative concentrations (10, 25, 50, 100, 500, 1000, 5000 ppm), using the optical configuration of Fig. 2(b) ($E_1 = 31$ mJ; $E_2 = 15$ mJ; $\Delta T = 72$ ns; $t_d = 700$ ns; $t_d = 1$ μs, = 35 μm). Figure 11 shows that varying concentrations of Ca are detectable at pressure and with a minimal change in inten-

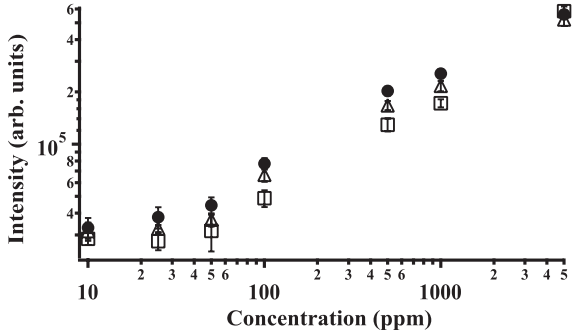

Fig. 11. Detection of Ca (422.673 nm) in a simulated vent fluid at varying pressures and concentrations. ● = 7×10^5 Pa, △ = 7×10^6 Pa, □ = 2.76×10^7 Pa.

sity suggesting that detection limits to the parts-per-million level will be obtainable at high pressure.

E. Solution Temperature Effects on Calcium Spectra

To characterize the temperature effects for Ca spectra, the sample cell was placed in a sand bath heated by a hot plate. The drainage port was removed and a thermocouple was inserted to record the temperature of the aqueous solution. We investigated the effect of temperature on the peak intensity of Ca(I) (422.673 nm) over the range of 27 °C–99 °C. Once the solution reached 99 °C, the hot plate was turned off and allowed to cool. Spectra were taken repeatedly using single-pulse LIBS as the temperature dropped. Ca line intensities were measured for a solution of 1000 ppm Ca and 2540 ppm NaCl at atmospheric pressure using a single laser pulse of 37 mJ (t_d = 100 ns, t_b = 1 μs, W = 35 μm), and the optical configuration shown in Fig. 2(c). Over this range, temperature had no effect on peak intensity.

4. Conclusions

An optimal range of low laser-pulse energies exists for the detection of Li, Ca, Mn, K, and Na in bulk aqueous solutions at both low and high pressures. No pressure effect was seen on the emission intensity for Ca and Na, and an increase in intensity with increased pressure was seen for Mn. No line broadening due to pressure was observed for Ca, Na, or Mn emission. A low-energy pulse may create a smaller, more tightly focused plasma that forms only at the focal spot. However, for a high-energy pulse, the high-energy density may cause breakdown even before the pulse reaches the focal spot. This may allow breakdown to occur over a longer distance. In addition, plasma shielding may occur. Further studies using imaging techniques will help to elucidate the relationship between the laser-pulse energy and the subsequent plasma that is formed. Using the dual-pulse technique for several analytes, a very short interpulse delay resulted in the greatest emission intensity. Since this condition approaches single-pulse conditions, dual-pulse LIBS may not be advantageous for some elements at high pressure. For different gate delays at fixed pressure, laser-pulse energy affects peak intensity. The addition of NaCl enhanced the emission intensity for Ca but had no effect on the intensity of Mn or K peaks. Ca was detectable over a wide range of concentrations and pressures. In addition, temperature changes below 99 °C had no noticeable effect on the emission intensity of Ca. Overall, increased pressure, the addition of NaCl to a solution, and temperature did not inhibit detection of analytes in solution. The results presented here suggest that LIBS is a viable technique for *in situ* chemical analysis in the deep ocean and further work should be carried out to develop LIBS into an *in situ* oceanographic sensor.

We acknowledge the National Science Foundation for support of this research under grants OCE0352278 and OCE0352242. Additional support was received from the Deep Ocean Exploration Institute of the Woods Hole Oceanographic Institution.

References

1. F. Brech and L. Cross, "Optical microemission stimulated by a a ruby MASER," Appl. Spectrosc. **16,** 59 (1962).
2. V. Majidi and M. Joseph, "Spectroscopic applications of laser-induced plasmas," Crit. Rev. Anal. Chem. **23,** 143–162 (1992).
3. L. Radziemski, "Review of analytical applications of laser plasmas and laser ablation, 1987–1994," Microchem. J. **50,** 218–234 (1994).
4. D. Rusak, B. Castle, B. Smith, and J. Winefordner, "Fundamentals and applications of laser-induced breakdown spectroscopy," Crit. Rev. Anal. Chem. **27,** 257–290 (1997).
5. K. Song, Y. Lee, and J. Sneddon, "Applications of laser-induced breakdown spectrometry," Appl. Spectrosc. Rev. **32,** 183–235 (1997).
6. J. Sneddon and Y. Lee, "Novel and recent applications of elemental determination by laser-induced breakdown spectroscopy," Anal. Lett. **32,** 2143–2162 (1999).
7. D. Rusak, B. Castle, B. Smith, and J. Winefordner, "Recent trends and the future of laser-induced plasma spectroscopy," Trend. Analyt. Chem. **17,** 453–461 (1998).
8. W. Lee, J. Wu, Y. Lee, and J. Sneddon, "Recent applications of laser-induced breakdown spectrometry: a review of material approaches," Appl. Spectrosc. Rev. **39,** 27–97 (2004).
9. B. Salle, J.-L. Lacour, E. Vors, P. Fichet, S. Maurice, D. A. Cremers, and R. C. Wiens, "Laser-induced breakdown spectroscopy for Mars surface analysis: capabilities at stand-off distances and detection of chlorine and sulfur elements," Spectrochim. Acta Part B **59,** 1413–1422 (2004).
10. Z. Arp, D. Cremers, R. D. Harris, D. Oschwald, G. R. Parker, Jr., and D. Wayne, "Feasibility of generating a useful laser-induced breakdown spectroscopy plasma on rocks at high pressure: preliminary study for a Venus mission," Spectrochim. Acta Part B **59,** 987–999 (2004).
11. W. Seyfried, Jr., K. Johnson, and M. C. Tivey, *In-situ sensors: their development and application for the study of chemical, physical and biological systems at mid-ocean ridges,* NSF/Ridge Sponsored Workshop Report (2000).
12. "The next generation of *in situ* biological and chemical sensors in the ocean: a workshop report," (2004). URL http://www.whoi.edu/institutes/OLI/activities/symposia_sensors.htm.
13. K. Daly, R. Byrne, A. Dickson, S. Gallager, M. Perry, and M. Tivey, "Chemical and biological sensors for time-series research: current status and new directions," Mar. Technol. Soc. J. **38,** 121–143 (2004).
14. T. Dickey, "The role of new technology in advancing ocean biogeochemical studies," Oceanography **14,** 108–120 (2001).
15. M. Varney, ed., *Chemical Sensors in Oceanography* (Gordon and Breach, 2000).
16. A. Pichahchy, D. Cremers, and M. Ferris, "Elemental analysis of metals under water using laser-induced breakdown spectroscopy," Spectrochim. Acta B **52,** 25–39 (1997).
17. P. Fichet, D. Menut, R. Brennetot, E. Vors, and A. Rivoallan, "Analysis by laser-induced breakdown spectroscopy of complex solids, liquids, and powders with an echelle spectrometer," Appl. Opt. **42,** 6029–6039 (2003).
18. P. Fichet, P. Mauchien, J.-F. Wagner, and C. Moulin, "Quantitative elemental determination in water and oil by laser induced breakdown spectroscopy," Anal. Chim. Acta **429,** 269–278 (2001).
19. G. Arca, A. Ciucci, V. Palleschi, S. Rastelli, and E. Tognoni, "Trace element analysis in water by the laser-induced breakdown spectroscopy technique," Appl. Spectrosc. **51,** 1102–1105 (1997).
20. O. Samek, D. Beddows, J. Kaiser, S. Kukhlevsky, M. Liska, H.

Telle, and J. Young, "Application of laser-induced breakdown spectroscopy to in situ analysis of liquid samples," Opt. Eng. **39,** 2248–2262 (2000).
21. J. Wachter and D. Cremers, "Determination of uranium in solution using laser-induced breakdown spectroscopy," Appl. Spectrosc. **41,** 1042–1048 (1987).
22. A. Kuwako, Y. Uchida, and K. Maeda, "Supersensitive detection of sodium in water with use of dual-pulse laser-induced breakdown spectroscopy," Appl. Opt. **42,** 6052–6056 (2003).
23. V. Rai, F. Yuch, and J. Singh, "Study of laser-induced breakdown emission from liquid under double pulse excitation," Appl. Opt. **42,** 2094–2101 (2003).
24. J.-S. Huang, C.-B. Ke, and K.-C. Lin, "Matrix effect on emission/current correlated analysis in laser-induced breakdown spectroscopy of liquid droplets," Spectrochim. Acta Part B **59**(3), 321–326 (2004).
25. X. Pu and N. H. Cheung, "ArF laser induced plasma spectroscopy of lead ions in aqueous solutions: plume reheating with a second Nd:YAG laser pulse," Appl. Spectrosc. **57,** 588–590 (1997).
26. W. Ho, C. Ng, and N. Cheung, "Spectrochemical analysis of liquids using laser-induced plasma emissions: effect of laser wavelength," Appl. Spectrosc. **51,** 87–91 (1997).
27. S. Nakamura, Y. Ito, and K. Sone, "Determination of an iron suspension in water by laser-induced breakdown spectroscopy with two sequential laser pulses," Anal. Chem. **68,** 2981–2986 (1996).
28. K. Lo and N. Cheung, "ArF laser-induced plasma spectroscopy for part-per-billion analysis of metal ions in aqueous solutions," Appl. Spectrosc. **56,** 682–688 (2002).
29. L. St-Onge, E. Kwong, M. Sabsabi, and E. Vadas, "Rapid analysis of liquid formulations containing sodium chloride using laser-induced breakdown spectroscopy," J. Pharm. Biomed. Anal. **36,** 277–284 (2004).
30. D. Cremers, L. Radziemski, and T. Loree, "Spectrochemical analysis of liquids using the laser spark," Anal. Chem. **38,** 721–729 (1984).
31. R. Knopp, F. Scherbaum, and J. Kim, "Laser induced breakdown spectroscopy (LIBS) as an analytical tool for the detection of metal ions in aqueous solutions," Fresenius J. Anal. Chem. **355,** 16–20 (1996).
32. W. Pearman, J. Scaffidi, and S. M. Angel, "Dual-pulse laser-induced breakdown spectroscopy in bulk aqueous solution with an orthogonal beam geometry," Appl. Opt. **42,** 6085–6093 (2003).
33. C. Hanisch, J. Liermann, U. Panne, and R. Niessner, "Characterization of colloidal particles by laser-induced plasma spectroscopy (LIPS)," Anal. Chim. Acta **346,** 23–25 (1997).
34. M. Noda, Y. Deguchi, S. Iwasaki, and N. Yoshikawa, "Detection of carbon in a high-temperature and high-pressure environment using laser-induced breakdown spectroscopy," Spectrochim. Acta **57,** 701–709 (2002).
35. M. Lawrence-Snyder, J. Scaffidi, S. M. Angel, A. P. M. Michel, and A. D. Chave, "Laser-induced breakdown spectroscopy of high-pressure bulk aqueous solutions," Appl. Spectrosc. **60,** 786–790 (2006).
36. C. Aragon, J. Aguilers, and J. Campos, "Determination of carbon content in molten steel using laser-induced breakdown spectroscopy," Appl. Spectrosc. **47,** 606–608 (1993).
37. J. Yun, R. Klenze, and J. Kim, "Laser-induced breakdown spectroscopy for the on-line multielement analysis of highly radioactive glass melt simulants: Part II. Analyses of molten glass samples," Appl. Spectrosc. **56,** 852–858 (2002).
38. A. Rai, F. Yueh, and J. Singh, "Laser-induced breakdown spectroscopy of molten aluminum alloy," Appl. Opt. **42,** 2078–2084 (2003).
39. L. Blevins, C. Shaddix, S. M. Sickafoose, and P. M. Walsh, "Laser-induced breakdown spectroscopy at high temperatures in industrial boilers and furnaces," Appl. Opt. **42,** 6107–6118 (2003).
40. K. Von Damm, "Chemistry of hydrothermal vent fluids from 9°–10°N, East Pacific Rise: 'time zero,' the immediate posteruptive period," J. Geophys. Res. **105,** 11203–11222 (2000).
41. D. A. Butterfield, I. R. Jonasson, G. J. Massoth, R. A. Feely, K. K. Roe, R. E. Embley, J. F. Holden, R. E. McDuff, M. D. Lilley, and J. R. Delaney, "Seafloor eruptions and evolution of hydrothermal fluid chemistry," Philos. Trans. R. Soc. A **355,** 369–386 (1997).
42. R. Noll, "Terms and notations for laser-induced breakdown spectroscopy," Anal. Bioanal. Chem. **385,** 214–218 (2006).
43. P. K. Kennedy, D. X. Hammer, and B. A. Rockwell, "Laser-induced breakdown in aqueous media," Prog. Quantum Electron. **21,** 155–248 (1997).
44. J. Brown, A. Colling, D. Park, J. Phillips, D. Rothery, and J. Wright, *Seawater: Its Composition, Properties and Behaviour* (The Open University, 1989).